Mixed quantum-classical versus full quantum dynamics: Coupled quasiparticle-oscillator system

Holger Schanz* and Bernd Esser
Institut für Physik, Humboldt-Universität, Invalidenstrasse 110, 10 115 Berlin, Germany
(Received 25 September 1996)

The relation between the dynamical properties of a coupled quasiparticle-oscillator system in the mixed quantum-classical and fully quantized descriptions is investigated. The system is considered as a model for applying a stepwise quantization. Features of the nonlinear dynamics in the mixed description such as the presence of a separatrix structure or regular and chaotic motion are shown to be reflected in the evolution of the quantum state vector of the fully quantized system. In particular, it is demonstrated how wave packets propagate along the separatrix structure of the mixed description, and that chaotic dynamics leads to a strongly entangled quantum state vector. Special emphasis is given to viewing the system from a dynamical Born-Oppenheimer approximation defining integrable reference oscillators, and elucidating the role of the nonadiabatic couplings which complement this approximation into a rigorous quantization scheme. [S1050-2947(97)05805-8]

PACS number(s): 03.65.−w, 05.45.+b, 31.30.Jv

I. INTRODUCTION

The relation between classical and quantum dynamics of nonlinear systems comprises specific aspects for systems treated in a mixed quantum-classical description. The correspondence between classical nonlinear systems on the one side and their fully quantized counterparts on the other has been intensively investigated in the last decade (see, e.g., [1–3]). In many systems relevant for molecular and condensed-matter physics, the direct quantization of the full system in one step is, however, not possible from a practical point of view. As a rule such systems divide naturally into interacting subsystems. Then a stepwise quantization is applied, resulting in a mixed description, in which one of the subsystems is treated in the quantum context and the other in the classical context. Furthermore, in complex systems the mixed description is often necessary for understanding global dynamical properties, e.g., the presence of bifurcations and separatrix structures dividing the solution manifold into characteristic parts, before for a selected energy region the full quantization can be performed.

This stepwise quantization is the basic idea on which the Born-Oppenheimer approximation [4] developed in the early days of quantum mechanics is based. Since then the separation of systems into subsystems, one treated classically and the other described in the quantum context, has been used in many situations. As examples we mention electronic spectra of molecules [5] or atomic and molecular collisions [6]. As is well known, this approximation can be complemented into a rigorous quantization scheme, if the nonadiabatic couplings are included [7]. These couplings can be the source of nonintegrability and chaos in the mixed quantum-classical description [8,9] and the problem of the quantum-classical correspondence arises for the dynamical properties of the mixed and fully quantized descriptions. The particular point we are stressing here is that chaos in the mixed description is produced by coupling one-dimensional integrable adiabatic reference states. This situation is different from the case where the main source of chaos lies in the dynamics on the adiabatic surfaces themselves when they support two or more dimensional vibronic motions, and the nonlinearity is strong enough to generate chaos [10].

In the present paper we consider the relation between the dynamical properties of the mixed and fully quantized descriptions for the particular model of a quasiparticle moving between two sites and coupled to an oscillator. Treating the oscillator in the classical or quantum contexts, whereas the quasiparticle moving between two sites is a quantum object from the beginning, one arrives at mixed and fully quantized levels of description. The coupled quasiparticle-oscillator system is an important model describing, e.g., excitons in molecular aggregates and coupled to vibrations [11]. It has also attracted widespread attention in the context of the spin-boson Hamiltonian and its quantum-classical phase space ([12–14] and references therein). Hence it seems appropriate to use this system as a model to analyze the relation between the mixed and fully quantized descriptions. We have recently investigated the dynamical properties of this model in the mixed description by integrating the corresponding Bloch-oscillator equations, and demonstrated the presence of a separatrix structure underlying the phase space for overcritical coupling, and of chaos developing from the hyperbolic point at the center of this structure. For increasing total energy, chaos spreads over the product phase space of the system constituted by the surface of the Bloch sphere and the oscillator plane [15]. Here we consider the problem of the relation between the dynamics in the mixed and fully quantum levels of description of the coupled quasiparticle-oscillator motion. Investigating this relation we focus on the adiabatic parameter range, where the mixed description is justified best, and hence the closest correspondence between the classical and quantum aspects of the oscillator dynamics can be expected. Although several aspects of the dynamics of the system have been considered previously [12,14], to our knowledge there exists no systematic investigation into the

*Present address: Max-Planck-Institut für Physik komplexer Systeme, Bayreuther Strasse 40, Haus 16, 01 187 Dresden, Germany. Electronic address: holger@mpipks-dresden.mpg.de

adiabatic parameter range that requires the numerical determination of a large number of eigenstates for the fully quantized system. The properties of these states and the corresponding eigenvalues were reported in [16]. In the present paper the dynamics of the fully quantized system is computed in order to compare the quantum evolution with the mixed description where the oscillator is treated classically. Performing this comparison, we use both fixed and adiabatic bases in the mixed description. The latter basis is of particular importance to clarify the role of the nonadiabatic couplings in the formation of the dynamics.

In Sec. II the model will be specified in detail. The mixed quantum-classical description is discussed in Sec. III, including the derivation of the equations of motion, the fixed point structure, and the dynamical properties of the system on this level of description. In Sec. IV the evolution of the fully quantized system is presented and compared to the dynamics in the mixed description. We demonstrate the effect of the separatrix structure in the mixed description on the oscillator wave packet propagation of the fully quantized version, dynamical subsystem correlations deriving from the separatrix structure and how the chaotic phase-space regions of the system in the mixed description show up in the nonstationary properties of the time dependent full quantum state vector.

II. MODEL

We consider a quasiparticle coupled to oscillator degrees of freedom. The quasiparticle is specified as a molecular exciton in a tight-binding representation, but can be substituted for by any other quantum object moving between discrete sites and described by a tight-binding Hamiltonian of the same structure. The system has the Hamiltonian

$$H^{(\mathrm{tot})}=H^{(\mathrm{exc})}+H^{(\mathrm{vib})}+H^{(\mathrm{int})}, \tag{1}$$

where $H^{(\mathrm{exc})}$, $H^{(\mathrm{vib})}$, and $H^{(\mathrm{int})}$ are the excitonic, vibronic, and interaction parts, respectively. $H^{(\mathrm{exc})}$ represents the quantum subsystem, which is taken in the site representation

$$H^{(\mathrm{exc})}=\sum_n \epsilon_n|c_n|^2+\sum_{n\neq m} V_{nm}c_n^*c_m, \tag{2}$$

where c_n is the quantum probability amplitude of the exciton to occupy the nth molecule with on-site energy ϵ_n, and V_{nm} the transfer-matrix element. For the intramolecular vibrations coupling to the exciton we use the harmonic approximation in $H^{(\mathrm{vib})}$,

$$H^{(\mathrm{vib})}=\frac{1}{2}\sum_n (p_n^2+\omega_n^2q_n^2). \tag{3}$$

Here q_n, p_n, and ω_n are the coordinate, the canonic conjugate momentum, and the frequency of the intramolecular vibration of the nth molecule, respectively. The interaction Hamiltonian $H^{(\mathrm{int})}$ represents the dependence of the exciton energy on the intramolecular configuration for which we use the first-order expansion in q_n,

$$H^{(\mathrm{int})}=\sum_n \gamma_n q_n|c_n|^2, \tag{4}$$

where γ_n are the coupling constants. The interaction is restricted to a single oscillator at each molecule. The simplest case of a symmetric two site system, e.g., an exciton in a molecular dimer constituted by two identical monomers, is considered in what follows. We set $\epsilon_1=\epsilon_2$, $\omega_1=\omega_2$, $\gamma_1=\gamma_2$ and $V_{12}=V_{21}=-V$, $V>0$. Then by introducing for the vibronic subsystem the coordinates and momenta

$$q_\pm=\frac{q_2\pm q_1}{\sqrt{2}}, \quad p_\pm=\frac{p_2\pm p_1}{\sqrt{2}}, \tag{5}$$

and for the excitonic subsystem the Bloch variables

$$x=\rho_{21}+\rho_{12}, \quad y=\mathrm{i}(\rho_{21}-\rho_{12}), \quad z=\rho_{22}-\rho_{11}, \tag{6}$$

where ρ_{mn} is the density matrix of the excitonic subsystem

$$\rho_{mn}=c_n^*c_m, \tag{7}$$

the relevant part of Eqs. (1)–(4) containing the vibration q_- is obtained in the form

$$H_-=-Vx+\frac{1}{2}(p_-^2+\omega^2q_-^2)+\frac{\gamma q_- z}{\sqrt{2}}. \tag{8}$$

The part corresponding to q_+ is not coupled to the exciton, and is omitted.

The Hamiltonian (8) can be represented as an operator in the space of the two-dimensional vectors $C=(c_1,c_2)$ constituted by the excitonic amplitudes c_n by using the standard Pauli spin matrices $\boldsymbol{\sigma}_i$ $(i=x,y,z)$. Passing in Eq. (8) to dimensionless variables by measuring H in units of $2V$ and replacing q_-, p_- by

$$Q=\sqrt{2V}q_-, \quad P=\frac{1}{\sqrt{2V}}p_-, \tag{9}$$

one finally obtains

$$\hat{\mathbf{H}}=-\frac{\boldsymbol{\sigma}_x}{2}+\frac{1}{2}(\hat{P}^2+r^2\hat{Q}^2)\mathbf{I}+\left(\frac{p}{2}\right)^{1/2}r\hat{Q}\boldsymbol{\sigma}_z, \tag{10}$$

with $\mathbf{I}$ denoting the 2×2 unit matrix.

$$p=\frac{\gamma^2}{2V\omega^2} \tag{11}$$

represents the dimensionless excitonic-vibronic coupling, and

$$r=\frac{\omega}{2V} \tag{12}$$

is the adiabatic parameter measuring the relative strength of quantum effects in both subsystems. We focus on the adiabatic case $r\ll1$, when the vibronic subsystem can be described in the classical approximation. The Hamiltonian (10) represents the simplest case of a spin-boson Hamiltonian (two quantum states coupled to one oscillator degree of freedom), and has been studied in various contexts before. Although Eq. (1) describes in general much more complicated

problems (more than two quantum states coupled to many oscillator degrees of freedom), we can use Eq. (10) to pinpoint the particular aspect of chaos due to nonadiabatic couplings in the mixed description.

III. MIXED QUANTUM-CLASSICAL DESCRIPTION

In this section we discuss the mixed quantum-classical dynamics resulting after a quasiclassical approximation to Eq. (10). It is instructive for this purpose to employ two representations differing in the basis set used for the excitonic part of the wave function. In the following two subsections the basic equations in these different representations are derived.

A. Fixed basis

In this case the basis states are given by the fixed molecule sites $|n\rangle$. Representing the excitonic state by $|\psi\rangle=\Sigma_n c_n|n\rangle$, inserting it into the time-dependent Schrödinger equation, and using Eq. (6) to replace the quantum amplitudes c_n by the Bloch variables, the quantum equations of motion for the excitonic subsystem describing the transfer dynamics between the two sites are obtained. The classical equations for the dynamics of the oscillator are found by using the expectation value of Eq. (10) as a classical Hamilton function from which the canonical equations for Q and P are derived. In this way one obtains the coupled Bloch-oscillator equations representing the dynamics of the system in the mixed description

$$\begin{aligned}\dot{x}&=-\sqrt{2p}rQy,\\ \dot{y}&=\sqrt{2p}rQx+z,\\ \dot{z}&=-y,\\ \dot{Q}&=P,\\ \dot{P}&=-r^2Q-\left(\frac{p}{2}\right)^{1/2}rz.\end{aligned}\tag{13}$$

Besides the energy

$$E=-\frac{x}{2}+\frac{1}{2}(P^2+r^2Q^2)+\left(\frac{p}{2}\right)^{1/2}rQz,\tag{14}$$

there is a second integral of the motion restricting the flow associated with the quantum subsystem to the surface of the unit radius Bloch sphere

$$R^2=x^2+y^2+z^2=1\,.\tag{15}$$

Sometimes it is advantageous to make use of this conserved quantity in order to reduce the total number of variables to four, e.g., when a formulation in canonically conjugate variables is also desired for the excitonic subsystem. One then introduces an angle ϕ by

$$x=\sqrt{1-z^2}\cos\phi,\quad y=\sqrt{1-z^2}\sin\phi.\tag{16}$$

We shall replace the usual Bloch variables by these coordinates where it is appropriate.

B. Adiabatic basis

In this case one first solves the eigenvalue problem of the part of the Hamiltonian (10) which contains excitonic operators

$$\mathbf{h}^{(\mathrm{ad})}=-\frac{\boldsymbol{\sigma}_x}{2}+\left(\frac{p}{2}\right)^{1/2}rQ\boldsymbol{\sigma}_z,\tag{17}$$

where Q is considered as an adiabatic parameter. The eigenvalues of Eq. (17) are given by

$$\epsilon_{\pm}^{(\mathrm{ad})}(Q)=\pm\tfrac{1}{2}w(Q),\tag{18}$$

where

$$w(Q)=\sqrt{1+2pr^2Q^2}.\tag{19}$$

The eigenvalues enter the adiabatic potentials for the slow subsystem

$$U_{\pm}^{(\mathrm{ad})}(Q)=\tfrac{1}{2}r^2Q^2+\epsilon_{\pm}^{(\mathrm{ad})}(Q).\tag{20}$$

The two eigenstates ($\alpha=1$ and 2) of Eq. (17) can be represented in the fixed basis as

$$|\alpha=1,Q\rangle=\frac{1}{\sqrt{2}}[+\sqrt{1+c(Q)}|1\rangle+\sqrt{1-c(Q)}|2\rangle]\tag{21}$$

and

$$|\alpha=2,Q\rangle=\frac{1}{\sqrt{2}}[+\sqrt{1-c(Q)}|1\rangle-\sqrt{1+c(Q)}|2\rangle],\tag{22}$$

with

$$c(Q)=\frac{\sqrt{2p}rQ}{w(Q)}\,.\tag{23}$$

The state vector of the excitonic subsystem can now be expanded in the adiabatic basis $|\psi\rangle=\Sigma_\alpha c_\alpha^{(\mathrm{ad})}|\alpha,Q\rangle$ and inserted into the time-dependent Schrödinger equation. In order to obtain the complete evolution equations in this basis, one has to take into account the time derivative of the expansion coefficients $c_\alpha^{(\mathrm{ad})}$ as well as the nonadiabatic couplings due to the time dependence of the states $|\alpha,Q(t)\rangle$ (the neglect of these couplings would result in the adiabatic approximation). Using $(d/dt)|\alpha,Q\rangle=\dot{Q}(d/dQ)|\alpha,Q\rangle$ the nonadiabatic coupling function

$$\varphi_{\alpha\beta}=\left\langle\alpha,Q\left|\frac{\partial}{\partial Q}\right|\beta,Q\right\rangle,\tag{24}$$

($\varphi_{\alpha\beta}=-\varphi_{\beta\alpha}$) is found, which in case of the eigenstates (21) and (22) is explicitly given by

$$\varphi_{12}=-\frac{\sqrt{p}r}{\sqrt{2}w^2(Q)}.\tag{25}$$

Introducing now in analogy to Eq. (6) the Bloch variables in the adiabatic basis, and treating the oscillator in the classical approximation, one obtains the coupled Bloch-oscillator equations in the adiabatic basis

$$\begin{aligned}
\dot{x}^{(\mathrm{ad})} &= 2P\varphi_{12}(Q)z^{(\mathrm{ad})} - w(Q)y^{(\mathrm{ad})},\\
\dot{y}^{(\mathrm{ad})} &= w(Q)x^{(\mathrm{ad})},\\
\dot{z}^{(\mathrm{ad})} &= -2P\varphi_{12}(Q)x^{(\mathrm{ad})},\\
\dot{Q} &= P,\\
\dot{P} &= -r^2Q + \sqrt{p}w(Q)\varphi_{12}x^{(\mathrm{ad})} - \left(\frac{p}{2}\right)^{1/2} rc(Q)z^{(\mathrm{ad})}.
\end{aligned} \tag{26}$$

The connection between the Bloch variables in the fixed and the adiabatic basis is given by

$$\begin{aligned}
x &= -c(Q)x^{(\mathrm{ad})} - \sqrt{1-c^2(Q)}z^{(\mathrm{ad})},\\
x^{(\mathrm{ad})} &= -c(Q)x - \sqrt{1-c^2(Q)}z\\
y &= -y^{(\mathrm{ad})}, \quad y^{(\mathrm{ad})} = -y\\
z &= c(Q)z^{(\mathrm{ad})} - \sqrt{1-c^2(Q)}x^{(\mathrm{ad})},\\
z^{(\mathrm{ad})} &= c(Q)z - \sqrt{1-c^2(Q)}x\\
\sqrt{1-z^2}\sin\phi &= -\sqrt{1-(z^{(\mathrm{ad})})^2}\sin\phi^{(\mathrm{ad})}.
\end{aligned} \tag{27}$$

Using these transformation formulas one can show that the equations of motion (13) derived in the fixed basis are actually equivalent to those in the adiabatic basis (26). The flow is again located on the surface of the unit Bloch sphere, and the energy can be expressed using the adiabatic Bloch variable $z^{(\mathrm{ad})}$ as

$$E = w(Q)\frac{z^{(\mathrm{ad})}}{2} + \frac{1}{2}(P^2 + r^2Q^2). \tag{28}$$

C. Fixed points and bifurcation

Essential information about the phase space of the excitonic-vibronic coupled dimer is contained in the location and stability properties of the fixed points of the mixed quantum-classical dynamics. Setting in the equations of motion in the fixed basis (13) all time derivatives to zero, for any stationary state we find

$$\begin{aligned}
Q_s &= -\frac{1}{r}\left(\frac{p}{2}\right)^{1/2} z_s, \quad P_s = 0, \quad y_s = 0\\
z_s &- px_sz_s = 0.
\end{aligned} \tag{29}$$

The stability properties of a fixed point are determined by a linearization of the equations of motion using canonical variables [15].

It is appropriate to subdivide all stationary points according to whether they are located in the bonding region $x_s > 0$ or in the antibonding region $x_s < 0$. There is no transition between these two groups when the parameters of the system are varied since $x_s = 0$ is excluded by Eq. (29). This terminology is in accordance with molecular physics, where it is common to refer to the state $x = 1$ with symmetric site occupation amplitudes $c_1 = c_2$ as bonding, and to the state $x = -1$ with antisymmetric amplitudes $c_1 = -c_2$ as antibonding.

1. Bonding region ($x_s > 0$)

We consider the bonding region first. The location of the fixed points is obtained from Eq. (29) using the additional restriction

$$x_s^2 + z_s^2 = 1\,. \tag{30}$$

One finds the following solutions in dependence on the value of the dimensionless coupling strength p:

(a) $0 \leqslant p \leqslant 1$: In this case Eq. (29) allows for a single solution only:

$$\mathbf{g}: \quad x_s = 1, \quad z_s = 0, \quad Q_s = 0, \quad E_s = -\tfrac{1}{2}\,. \tag{31}$$

This point is the bonding ground state corresponding to a symmetric combination of the excitonic amplitudes $c_1 = c_2 = 1/\sqrt{2}$. **g** is stable elliptic.

(b) $p \geqslant 1$: A bifurcation has occurred and we obtain three stationary points:

$$\begin{aligned}
\mathbf{g}_{\pm}: \quad & x_s = \frac{1}{p}, \quad z_s = \pm\frac{\sqrt{p^2-1}}{p}\,,\\
& Q_s = \pm\frac{\sqrt{p^2-1}}{\sqrt{2p}r}, \quad E_s = -\frac{p^2+1}{4p}.
\end{aligned} \tag{32}$$

These two points are stable elliptic.

$$\mathbf{h}: \quad x_s = 1\,, \quad z_s = 0, \quad Q_s = 0, \quad E_s = -\tfrac{1}{2}\,. \tag{33}$$

The point **h** is at the position of the former ground state, but in contrast to **g** it is unstable hyperbolic.

Hence the parameter p governs a pitchfork bifurcation: The ground state **g** below the bifurcation ($p < 1$) splits into two degenerate ground states $\mathbf{g}_{\pm}$ above bifurcation ($p > 1$). At the former ground state a hyperbolic point **h** appears. This situation is also obvious from Fig. 1(a).

2. Antibonding region ($x_s < 0$)

Independent on the coupling strength p we have in this region only one solution of Eq. (29) [see Fig. 1(b)]:

$$\mathbf{e}: \quad z_s = 0, \quad x_s = -1, \quad Q_s = 0, \quad E_s = +\tfrac{1}{2}\,. \tag{34}$$

This stationary state corresponds to an antisymmetric combination of the excitonic amplitudes $c_1 = -c_2 = 1/\sqrt{2}$. **e** is stable for

$$\frac{|r^2-1|}{r} > 2\sqrt{p}, \tag{35}$$

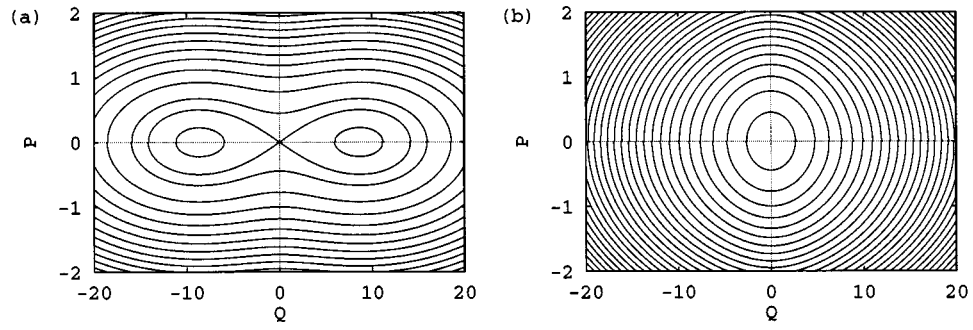

FIG. 1. Phase-space plots for the adiabatic oscillators (left: lower potential, right: upper potential) for $p=2$ and $r=0.1$.

which holds when the system is not in resonance, and in particular for the adiabatic case $r \ll 1$.

Since the equations of motion in fixed and in adiabatic bases are equivalent, it is clear that the same fixed points (29) can also be obtained from Eq. (26). Setting the time derivatives of x, y, and Q in Eq. (26) equal to zero, for the stationary states one finds

$$x_s^{(\mathrm{ad})}=0, \quad y_s^{(\mathrm{ad})}=0, \quad P_s^{(\mathrm{ad})}=0, \tag{36}$$

leaving for $z_s^{(\mathrm{ad})}$ only the two values

$$z_s^{(\mathrm{ad})}=\pm 1\,. \tag{37}$$

The equation $\dot{P}=0$ reduces to

$$[w(Q)+pz_s^{(\mathrm{ad})}]Q=0\,. \tag{38}$$

For $z_s^{(\mathrm{ad})}=+1$ the only solution of Eq. (38) is $Q_s=0$, whereas for $z_s^{(\mathrm{ad})}=-1$ one obtains additional solutions for $p>1$. These solutions are easily seen to correspond to the bifurcation discussed above.

It is worth noting that in the adiabatic basis the stationary states are always located at $z_s^{(\mathrm{ad})}=\pm 1$, and that this will be the case for any system treated in mixed quantum-classical description and restricted to the lowest two adiabatic levels. A specific feature of using the adiabatic basis is the independence of the location of the fixed points on the explicit form of the nonadiabatic coupling function, since this function enters the equations of motion in form of the products $\varphi_{12}(Q)P$ and $\varphi_{12}(Q)x^{(\mathrm{ad})}$ which drop out at a fixed point because of Eq. (36). From Eq. (27) it is, moreover, easy to see that the fixed points in the bonding region are located within the lower adiabatic potential, while the antibonding fixed points belong to the upper one.

D. Integrable approximations

Before we investigate the dynamics of the complete coupled equations of motion (13) or (26) we would like to mention two integrable approximations to the model. The first, trivial integrable approximation is to set in the equations of motion in the fixed basis (13), $p=0$, which results in a decoupling of the excitonic and vibronic motions. The second and more interesting integrable approximation is obtained by neglecting the nonadiabatic coupling function φ_{12} in the equations of motion (26) in the adiabatic basis. One obtains the dynamics of the decoupled one-dimensional adiabatic oscillators corresponding to the Hamiltonians

$$h_{\pm}^{(\mathrm{ad})}=\tfrac{1}{2}P^2+U_{\pm}^{(\mathrm{ad})}(Q), \tag{39}$$

where $U_{\pm}^{(\mathrm{ad})}(Q)$ is given by Eq. (20). In this approximation some of the nonlinear features of the model are still contained in the integrable adiabatic reference oscillators, Eq. (39). In particular the lower adiabatic potential (20) displays the bifurcation from a single minimum structure to the characteristic double-well structure when the parameter p passes through the bifurcation value $p=1$. Formally the neglect of φ_{12} does not necessarily lead to $z_s^{(\mathrm{ad})}=\pm 1$: According to the equations of motion (26), $\varphi_{12}=0$ implies $z_s^{(\mathrm{ad})}=\mathrm{const}$. Then in the dynamics of the adiabatic approximation both adiabatic modes can be occupied, and only the transitions between them are switched off. The oscillator equations become autonomous describing regular motion according to the classical Hamilton function (28), with $z_s^{(\mathrm{ad})}$ a parameter. The oscillator coordinate $Q(t)$ enters the Bloch equations for $x(t)$ and $y(t)$. The equations for the latter describe the regular motion on a circle generated by an intersection of the Bloch sphere with the plane $z_s^{(\mathrm{ad})}=$ const, on which the phase oscillations between the modes are realized. The regular phase space structures following from the integrable adiabatic reference oscillators (39) above the bifurcation are shown in Fig. 1.

In the following we demonstrate that the regular structures associated with the adiabatic approximation are present in both the mixed and fully quantized descriptions. At the same time we show that the complete coupled system of Bloch-oscillator equations, i.e., including the nonadiabatic couplings, displays dynamical chaos. This identifies the nonadiabatic couplings as a source of nonintegrability and chaos in the mixed description of the system, and raises a question about the signatures of this chaos after full quantization is performed. The latter problem will be addressed in Sec. V.

E. Dynamical properties

The dynamical properties of the coupled Bloch-oscillator equations (13) were analyzed by a direct numerical integration. Some of our results, such as the presence of chaos in the mixed description of the excitonic-vibronic coupled dimer, were already reported in [15]. Therefore the aim of this section is twofold: On the one side we reconsider the findings in [15] relating the dynamical structures to the adiabatic approximation, in which the integrable reference systems (39) can be defined. This clarifies the role of the nonadiabatic couplings in the formation of the dynamics of the model,

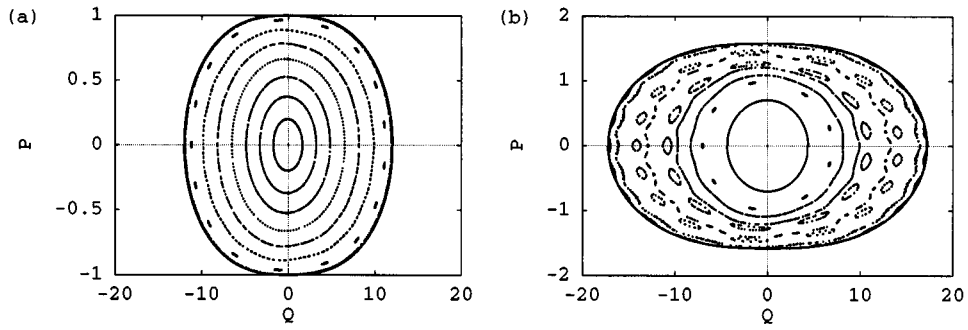

FIG. 2. Poincaré section in the oscillator variables for $p=0.8$ (below bifurcation), $r=0.1$ and (a) $E=0.0$ and (b) $E=0.75$. The Bloch variable y is fixed ($y=0$, $dy/dt>0$).

which was not done before. On the other side we give the necessary characterization of the phase-space structure, such as the regions and associated parameters belonging to the regular and chaotic parts of the dynamics, respectively. This will provide the basis to perform the comparison of the mixed description with the full quantum evolution in Sec. IV.

We used the fixed basis for the integration of the equations of motion in the mixed description, since it is numerically more convenient. In view of the existence of two integrals of the motion, only three from the total of five variables of the system are independent. Therefore a standard two-dimensional Poincaré surface of section can be defined for both the oscillatory and excitonic subsystems by fixing one variable. In Fig. 2(a) a Poincaré section in oscillator variables is presented for the value $p=0.8$, which is below the bifurcation value $p=1$. In this case the adiabatic potential $U_-(Q)$ has a single minimum. The total energy is fixed at $E=0$, i.e., well below the minimum of the upper adiabatic potential. Therefore the influence of this potential is small, and the oscillator dynamics can be expected to be close to the regular dynamics of the lower reference oscillator associated with $U_-(Q)$. This is indeed confirmed by Fig. 2(a). There is, however, a chain of small resonance islands in the outer part of the surface of section, which is due to resonance between the oscillator motion and the occupation oscillations between the adiabatic modes. The interaction between the occupation oscillations due to the finite $\dot{z}^{(\mathrm{ad})}$ and the oscillator motion becomes much more pronounced for higher energies. A corresponding Poincaré section is displayed in Fig. 2(b) for the same value $p=0.8$ of the coupling constant, but with the energy now chosen above the minimum of the upper adiabatic potential. This choice of the energy allows according to Eq. (28) a much broader range for the variation of the variable $z^{(\mathrm{ad})}$, and consequently the nonadiabatic couplings are more effective. Correspondingly we now observe several resonance chains.

Increasing the coupling above the bifurcation value $p=1$, but fixing the total energy below E_h, one expects regular oscillations around the displaced minima of the double-well structure in $U_-(Q)$. A Poincaré section in the oscillator variables corresponding to this behavior is shown in Fig. 3(a). Increasing the energy to a value slightly above E_h [Fig. 3(b)], one finds Poincaré sections resembling the separatrix structure as shown in Fig. 1(a).

For energies well above E_h many chaotic trajectories do exist. Characteristic examples are provided by the Poincaré

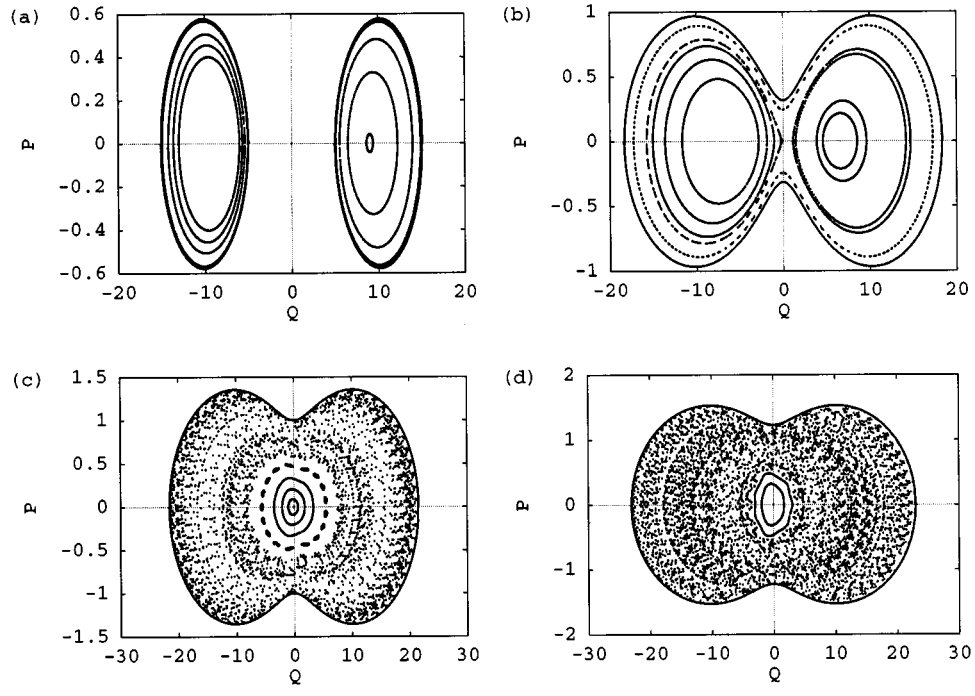

FIG. 3. Poincaré sections in the oscillator variables for $p=3.4$ (above bifurcation), $r=0.1$ and (a) $E=-0.75$, (b) $E=-0.45$, (c) $E=0.0$ and (d) $E=0.25$. The Bloch variable y is fixed ($y=0$, $dy/dt>0$).

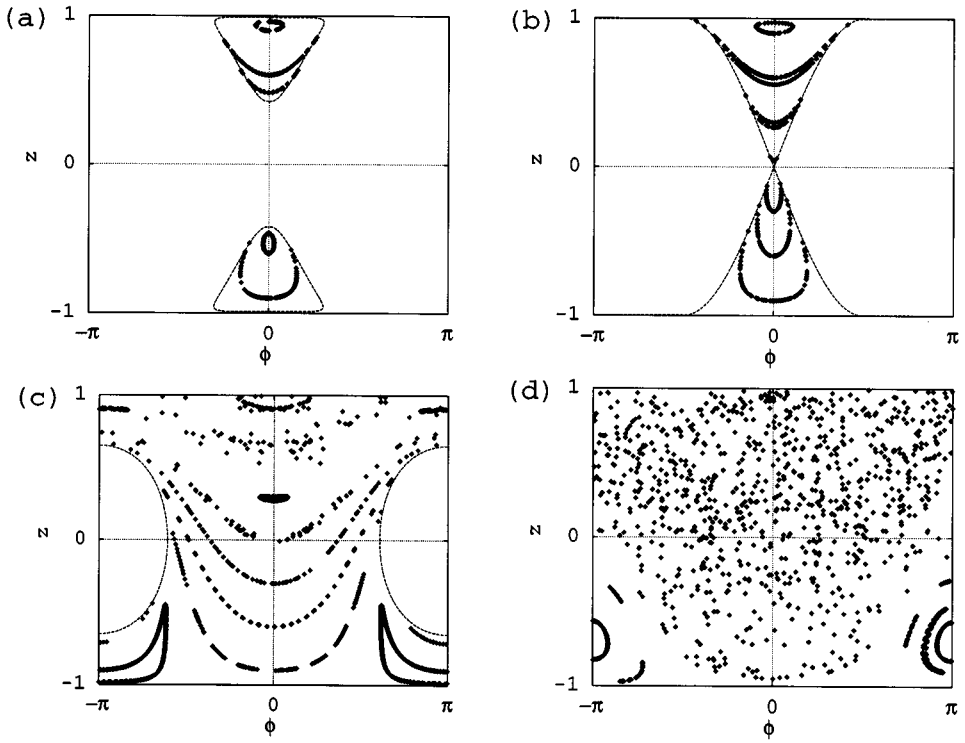

FIG. 4. Poincaré section in the excitonic variables for $r=0.1$, $p=2.0$ (above bifurcation) and different energies: (a) $E=-0.54$, (b) $E=-0.5$, (c) $E=+0.5$, and (d) $E=0.83$ (see also Fig. 8). The surface of the section is defined by the left-turning point of the oscillator ($P=0$, $dP/dt>0$), and displayed using the coordinates z and ϕ (note the periodicity of the abscissa).

sections in oscillator variables displayed in Figs. 3(c) and 3(d) with the total energy of case (c) below that of case (d). It is seen how the regular part of the oscillator phase space becomes smaller, and the chaotic part grows with increasing energy. The destruction of the regular dynamics is seen to be connected mainly with the energy of the vibronic subsystem: Regular dynamics is restricted to the inner region of the Poincaré sections, i.e., to oscillator states with low-energy, small-amplitude oscillations and consequently small effective coupling, whereas high oscillator energy corresponding to the outer regions in Figs. 3(c) and 3(d) results in chaos.

The dynamics of the oscillator subsystem is complemented by the Poincaré sections on the surface of the Bloch sphere showing the behavior of the excitonic subsystem. In Figs. 4(a)–4(d) a typical set of Poincaré sections is presented for different energies and above the bifurcation. The sections correspond to the left-turning point of the oscillator. For low energy one again finds regular dynamics in the region of the bifurcated ground states. These trajectories represent self-trapped solutions of the system in which the exciton is preferentially at one of the sites of the dimer and correspond to the one-sided oscillations of the vibronic subsystem in Fig. 3(a). In the vicinity of the hyperbolic point E_h, local chaos starts to develop. This can be considered a perturbation due to nonadiabatic couplings of the dynamics near the saddle of the lower adiabatic potential $U_-(Q)$. With increasing energy, chaos spreads over the Bloch sphere, leaving only regular islands in the region of antibonding states associated with the upper adiabatic potential and in accordance with the dynamics of the vibronic subsystem discussed above. For high enough energy the coupling between the adiabatic reference oscillators almost completely destroys regular structures and results in global chaos.

IV. QUANTUM EVOLUTION

Treating in Hamiltonian (10) the coordinate $\hat{Q}$ and the momentum $\hat{P}$ as noncommuting quantum operators, we now turn to the full quantum dynamics of the model. We focus on the features of the evolution in the adiabatic parameter region $r \ll 1$. The evolution of the full quantum state vector of the system satisfying some specified initial condition is computed using the eigenstate representation of the Hamiltonian. The diagonalization of Hamiltonian (10) was performed using a large set of oscillator eigenfunctions for the undisplaced oscillator as a basis, i.e., the basis was constructed from the product states $|n,\nu\rangle = |n\rangle \otimes |\nu\rangle$, where the index n labels the two sites of the dimer, and $\nu = 0,1,\ldots$ stands for the oscillator quantum number. In this basis the Hamiltonian (10) is represented by the matrix

$$\langle n,\nu|\hat{\mathbf{H}}|n',\nu'\rangle$$

$$= -\frac{[1-(-1)^{\nu+\nu'}]}{4}\delta_{\nu,\nu'} + r(\nu+\tfrac{1}{2})\delta_{n,n'}\delta_{\nu,\nu'}$$

$$+ \sqrt{\frac{pr}{2}}(-1)^n(\sqrt{\nu'}\,\delta_{\nu,\nu'-1} + \sqrt{\nu}\,\delta_{\nu,\nu'+1})\delta_{n,n'}. \quad (40)$$

The typical number of oscillator eigenfunctions used was 750, yielding a total of 1500 basis states. The properties of the stationary eigenstates, the fine structure of the spectrum, and in particular the role of the adiabatic reference oscillators and the nonadiabatic couplings in the formation of the spectrum were reported in [16]. Here we consider the nonstationary properties of the full quantum system based on this eigenstate expansion, and demonstrate how the nonlinear

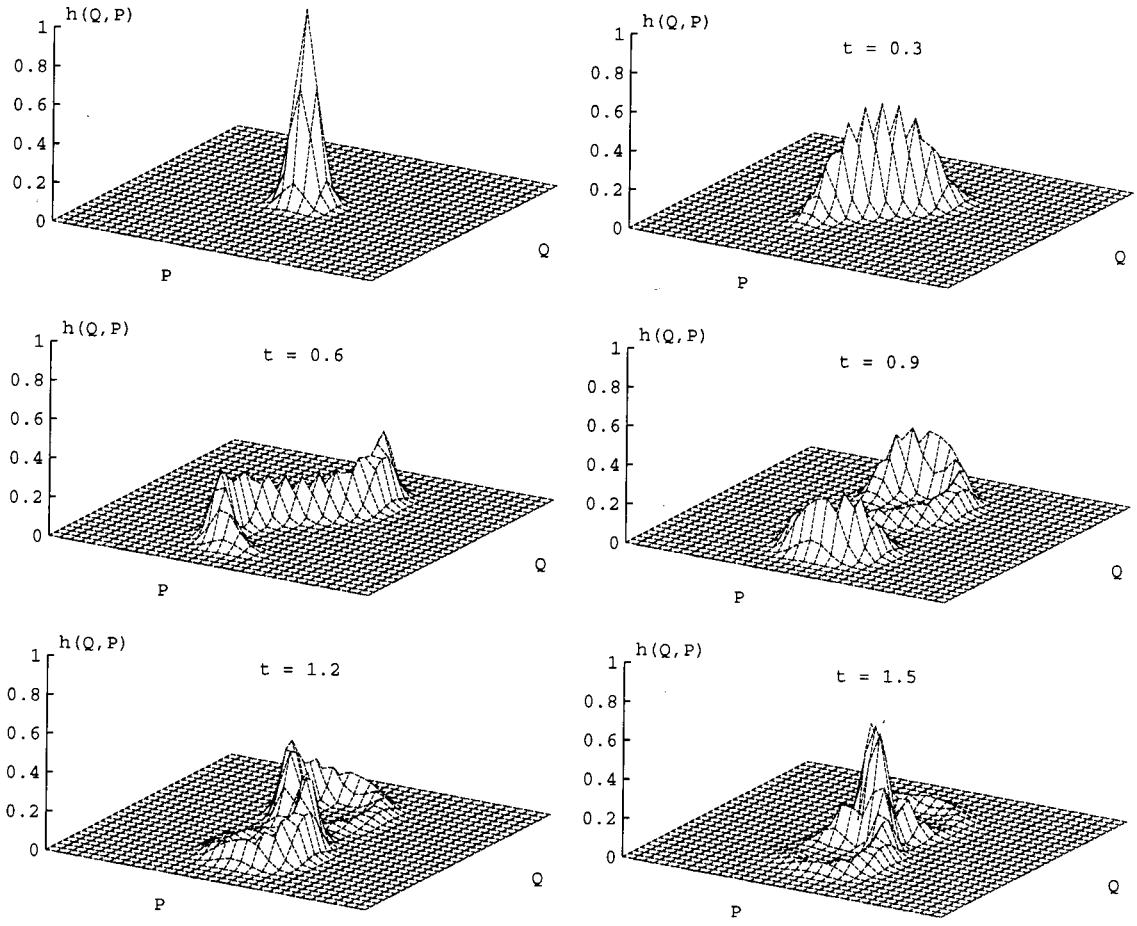

FIG. 5. Evolution of a Gaussian wave packet initially located at the hyperbolic fixed point for $p=2$ and $r=0.01$. Husimi distribution (43) for the wave function projected on the excitonic states $z=0$ and $\phi=0$ in a surface plot.

features of the dynamics in the mixed quantum-classical description are reflected in the time dependence of the full quantum state vector $|\Psi(t)\rangle$.

We investigated the evolution of wave packets initially prepared in the product state

$$|\Phi,\alpha\rangle=|\Phi_{z_0,\phi_0}\rangle\otimes|\alpha_{Q_0,P_0}\rangle, \tag{41}$$

where Φ is an excitonic two component wave function which is specified up to an irrelevant global phase by the expectation values of the Bloch variables z and ϕ [see Eqs. (6) and (16)]. The complex parameter

$$\alpha(Q,P)=\left(\frac{r}{2}\right)^{1/2}\langle\alpha|\hat{Q}|\alpha\rangle+\frac{\mathrm{i}}{\sqrt{2r}}\langle\alpha|\hat{P}|\alpha\rangle \tag{42}$$

labels a standard coherent state in the oscillator variables.

In order to map the evolution of the full state vector $|\Psi(t)\rangle$ constructed from the eigenstate expansion according to the initial condition (41) onto an analog of the phase space of the mixed description, in which the oscillator is treated classically, for the oscillator subsystem we used the Husimi distribution, which is an appropriate quantum analog to the classical phase-space distribution (see, e.g., [17]). It is defined by projecting $|\Psi(t)\rangle$ on the manifold of coherent states

$$h_{z,\phi}(Q,P)=|\langle\Phi_{z,\phi},\alpha_{Q,P}|\Psi(t)\rangle|^2, \tag{43}$$

where now Q and P are varied in the oscillator plane, while z and ϕ are fixed parameters.

Without the interaction between the subsystems a wave packet prepared in a coherent oscillator state would travel undistorted along the classical trajectory started at (Q_0,P_0). A weak coupling below the bifurcation ($p<1$) results in a similar picture (not displayed) with the wave packet after some initial period almost uniformly covering the classical trajectories such as those displayed in Figs. 2(a) and 2(b).

Of particular interest is the effect of the separatrix structure characterizing the mixed description above the bifurcation ($p>1$) on the propagation of the oscillator wave packet. For a system with a proper classical limit and a separatrix in the classical phase space, the correspondence to the quantum evolution was studied, e.g., in [3]. Similar to this we found that the presence of the separatrix is clearly reflected in the wave-packet dynamics when the energy is fixed at E_h. In Fig. 5 the evolution of a quantum state prepared initially right at the hyperbolic fixed point **h** is presented. The rel-

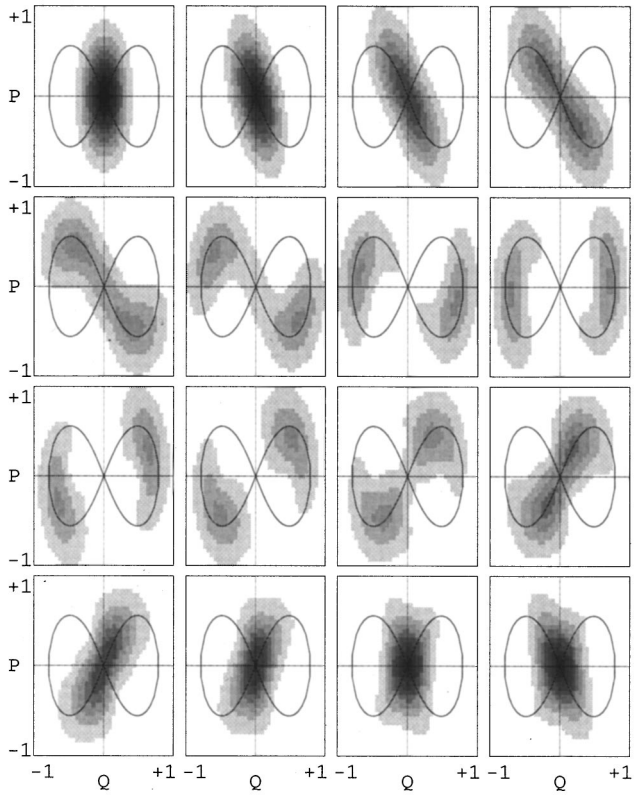

FIG. 6. Evolution of a quantum state prepared at $t=0$ as a Gaussian wave packet on the hyperbolic fixed point of the mixed quantum-classical dynamics ($p=2$, $r=0.1$, and $\delta t=0.1$). The state is represented by the corresponding Husimi distribution after projection on the excitonic state $z=0$, $\phi=0$. The value of the Husimi distribution is encoded by the color using a linear scale with white corresponding to zero, and black to 1. The solid line is the isoenergy line of the lower adiabatic potential at the energy of the wave packet ($E=-0.5$), i.e., the separatrix associated with the hyperbolic fixed point in the adiabatic approximation.

evant parameters are $p=2$ and $r=0.01$ and the Husimi distribution (43) for the projection onto the excitonic states $z=0$ and $\phi=0$ is displayed. It is seen how the oscillator wave packet spreads along the unstable direction of the separatrix structure. The asymmetric distortion of the wave packet in the beginning of the propagation, when the support of the Husimi distribution is given by the unstable direction of the separatrix, is remarkable.

In Fig. 6 contour plots for an analogous wave packet propagation started at the hyperbolic point but for a larger adiabatic parameter $r=0.1$ are presented. The propagation along the separatrix structure, which is shown by a full line, is again evident. This indicates that the well-known quantum-classical correspondence in the case of regular dynamics, namely, that the quantum distribution follows the flow of the classical system, can be extended to systems treated in a mixed quantum-classical description. A more detailed comparison of the results for $r=0.01$ (Fig. 5) and $r=0.1$ (Fig. 6) reveals, as expected, that the width of the wave-packet transversal to the underlying classical structure is reduced as the system is closer to the adiabatic limit. We conclude that in the adiabatic regime regular structures such as a separatrix in the formally classical phase space of the mixed description can serve to forecast qualitatively the evolution of a wave packet in the fully quantized system.

In Fig. 7 we compare the Husimi distributions for one and the same wave packet projected onto two different excitonic states in order to reveal the quantum correlations between the excitonic and the vibronic subsystems. In Fig. 7(a) we chose $z=0$ and $\phi=0$ corresponding to equal site occupation probabilities, whereas in Fig. 7(b) the wave packet is projected onto $z=1$, i.e., an excitonic state completely localized at one of the dimer sites. It is seen that for the case of an equal site occupation the oscillator covers both branches of the separatrix structure, whereas for the one sided projection the oscillator is preferentially located on the branch of the separatrix corresponding adiabatically to the occupied site. This behavior reflects the the property of the quantum system to include coherently all the variants of motion of the mixed quantum-classical system weighted with the corresponding probability in resemblance to the semiclassical propagator of a system with proper classical limit, which is given as a sum over classical trajectories.

The demonstrated correlations between the two subsystems imply that the total wave function cannot be factorized into a product of subsystem wave functions. This factorization is, however, the basic assumption the mixed quantum-classical description is based upon. Hence the agreement between the mixed description and the full quantum evolution of expectation values deteriorates as the coupling parameter p is increased beyond the bifurcation value $p=1$, where strong subsystem correlations start to appear. In a similar way the mixed description can be expected to fail, whenever the system shows a bifurcation. In fact a bifurca-

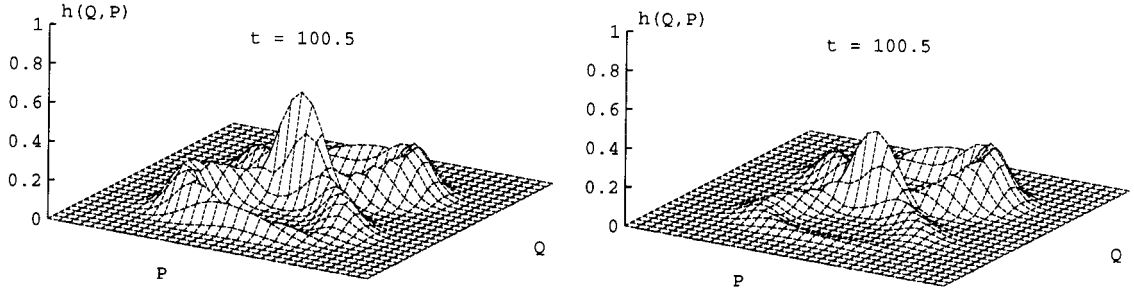

FIG. 7. Form of a Gaussian wave packet initially located at the hyperbolic fixed point for $p=2$ and $r=0.01$ at large time. Husimi distribution of the wave function projected on the excitonic states $z=0$ and $\phi=0$ (left), and $z=1$ (right) in a surface plot.

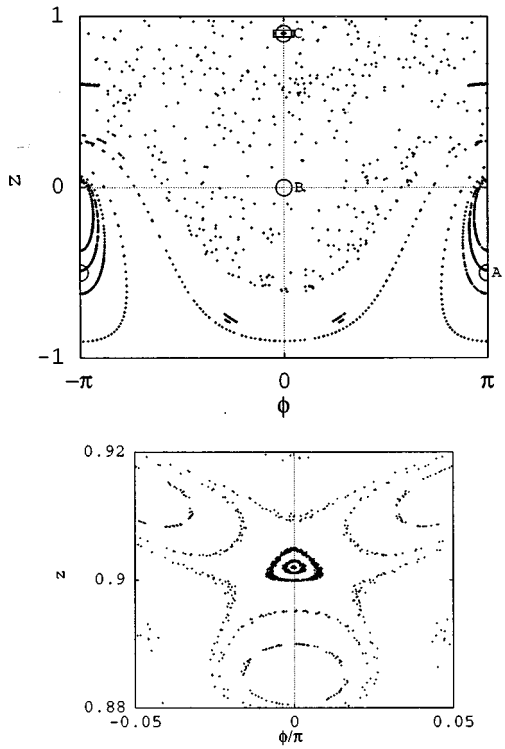

FIG. 8. Poincaré section $P=0$, $dP/dt>0$ for the symmetric dimer with $r=0.1$ and $p=2$ at $E=+0.5$. The circles mark the initial states, for which the time evolution will be displayed in the following figures. A regular island embedded into the chaotic sea has been enlarged in the lower part of the figure.

tion is only one way to produce nonlocalized wave packets with correlations between the subsystems. Even stronger correlations can be expected when wave packets are prepared in chaotic regions of the mixed quantum-classical phase space where the instability of classical trajectories is global and not restricted to a hyperbolic fixed point. In the remainder we will address the problem of how this property is reflected in the evolution of the fully quantized system.

For systems quantized in one step and chaotic in the classical limit the differences in the quantum evolution between initial conditions selected in the regular and chaotic parts of the classical phase space of the system are well known: If the initial conditions of the quantum system are selected in the regular part of the classical phase space the time dependence of the appropriately chosen quantum expectation values follow the corresponding classical values over a substantial amount of time, whereas for initial conditions chosen in the chaotic part of the classical phase space these values start to deviate from each other almost immediately (see, e.g., [18]). In order to investigate this connection in our case we have selected different initial conditions in the regular and chaotic parts of the Bloch sphere of the system, and compared the evolution in the mixed description with that of expectation values obtained from the fully quantized system. In Fig. 8 three different initial conditions on the Bloch sphere of the excitonic subsystem are shown. **A** belongs to the main regular region of the dynamics in the mixed description, **B** to the chaotic region, and **C** to a small regular island embedded in a large chaotic surrounding. For a comparison of the dynamics in the mixed and fully quantized descriptions for these cases we selected the variables $Q(t)$ and $z(t)$ displayed in the upper parts of Figs. 9–11.

We first compare the dynamics for initial conditions located in the main regular (antibonding) and main chaotic (bonding) regions. Since the initial state of the fully quantized system is chosen as a product state for which the decoupling implicit in the derivation of Eq. (13) is justified, there is always an interval at the beginning of the time evolution where the mixed description follows closely the quantum data. Then, however, there is indeed a striking difference between initial conditions selected in the regular and the chaotic parts of the phase space of the mixed system: For initial conditions in the regular part (**A**, Fig. 9) the quantum expectation value $Q(t)$ follows the classical trajectory of the

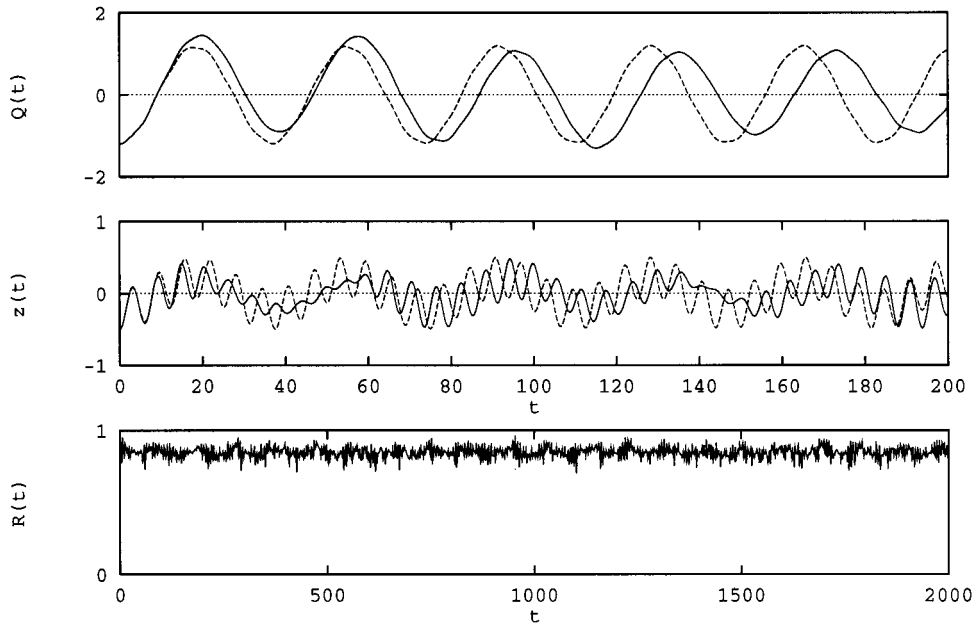

FIG. 9. Time evolution of the initially factorized coherent state corresponding to **A** in Fig. 8 [$\phi(t=0)=\pi$, $z(0)=-0.5$, $Q(0)=-1.2$, $E=0.55$]. In the upper parts the quantum expectation values of Q and σ_z (full lines) are compared to the corresponding quantities of the mixed quantum-classical description (dashed lines). In the lower part the quantum Bloch radius $R(t)$ (44) is displayed using a larger time scale.

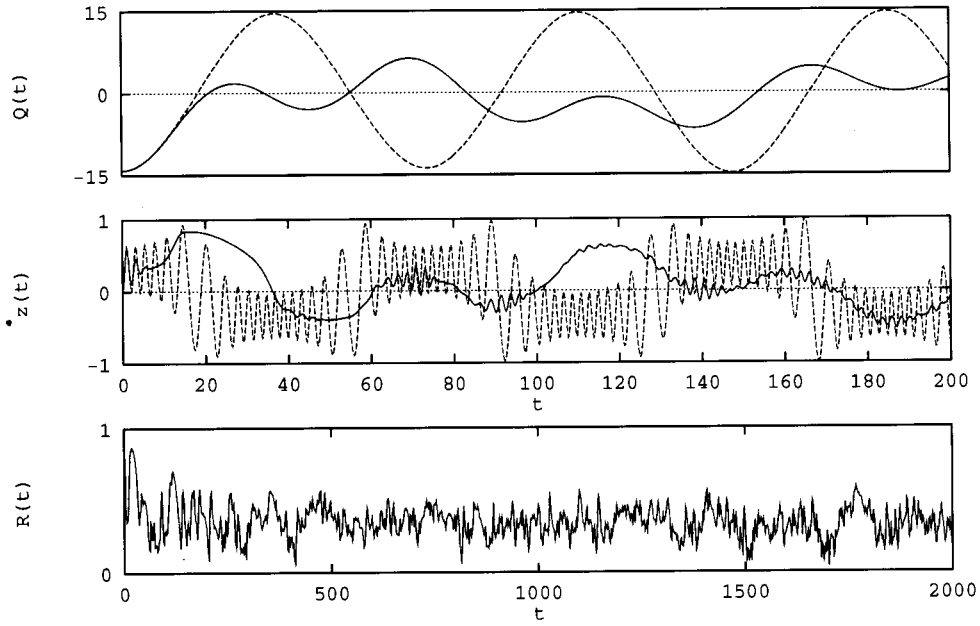

FIG. 10. Time evolution of the initially factorized coherent state corresponding to **B** in Fig. 8 [$\varphi(\tau=0)=0$, $z(0)=0$, $Q(0)=-14.1$, $E=0.55$]. See Fig. 9 for details.

mixed description over several periods and then, apart from a slowly growing phase shift, both dependences keep a similar oscillatory form, whereas for an initial condition in the chaotic part (**B**, Fig. 10) the corresponding curves are completely different and the deviation between both starts already after a fourth of the oscillator period. This confirms for our case the general feature of classically chaotic systems to produce a fast breakdown of the validity of quasiclassical approximations. The comparison for the occupation difference $z(t)$ of the excitonic sites is not so direct, because the exciton constitutes the fast subsystem displaying rapid oscillations in the mixed description. For the regular case we observe that the slowly changing mean value of $z(t)$ obtained from the mixed description is related to the quantum data, though the amplitude and phase of the superimposed rapid oscillations are different after a few periods of the excitonic subsystem. In the chaotic case the breakdown of the mixed description for shorter times is evident and there is no correspondence for the mean values.

The gradual development of quantum correlations between both subsystems, which are absent in the initially factorized state, can be quantified by calculating the effective Bloch radius

$$R(t)=\sqrt{x^2(t)+y^2(t)+z^2(t)} \tag{44}$$

of the excitonic subsystem using the time-dependent expectation values of $\boldsymbol{\sigma}_x$, $\boldsymbol{\sigma}_y$, and $\boldsymbol{\sigma}_z$. Note that the reduced density matrix $\rho(t)$ for the excitonic subsystem, obtained from the full density matrix by taking the trace over the

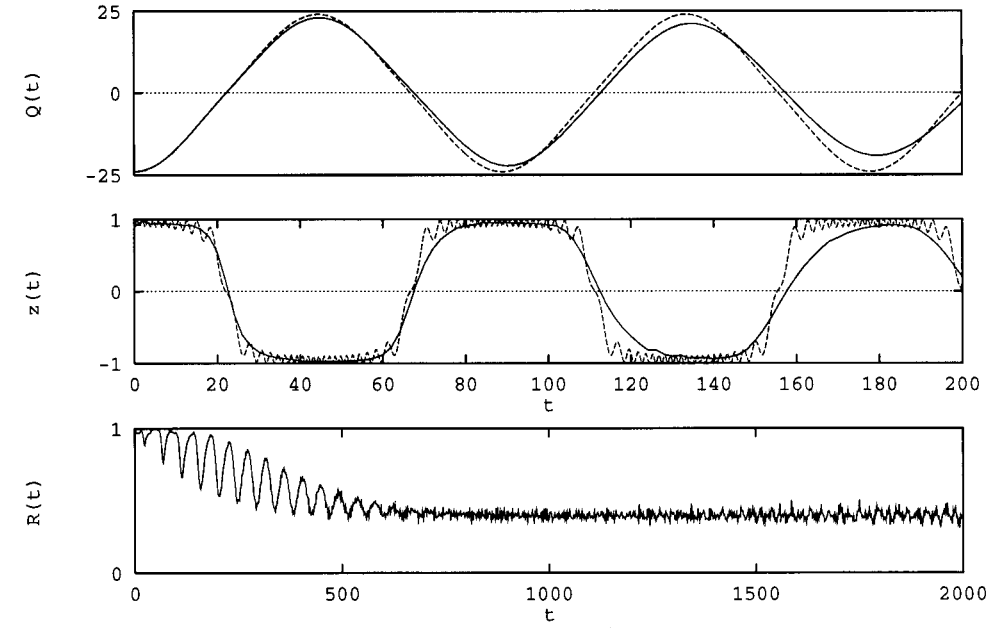

FIG. 11. Time evolution of the initially factorized coherent state corresponding to **C** in Fig. 8 [$\varphi(\tau=0)=0$, $z(0)=0.9$, $Q(0)=-24.0$, $E=0.55$]. See Fig. 9 for details.

oscillator states, is related to $R(t)$ via $\mathrm{Tr}\rho^2(t) = \frac{1}{2}[1+R^2(t)]$. For the factorized and correspondingly uncorrelated initial quantum state the value of the Bloch radius is $R(0)=1$. $R(t)$ will decrease in the course of time according to the degree to which quantum correlations lead to an entanglement between both subsystems. In the lower parts of Figs. 9–11, the dependence of the Bloch radius on the time is displayed for a long-time interval. The difference between the behavior for initial conditions chosen in the regular and chaotic parts of the phase space of the mixed description is remarkable: For initial conditions in the regular part of the phase space $R(t)$ stabilizes at a value close to 1, whereas for the initial conditions in the chaotic part the descent is much more pronounced, and the long-time value of $R(t)$ is much lower, thus indicating stronger quantum correlations in the chaotic case. The correlations between the subsystems are the reason for the breakdown of the mixed description which implicitly contains the factorization of expectation values. Therefore the smaller value of $R(t)$ observed for the state prepared in the chaotic region confirms the faster breakdown of the mixed description as compared to a regular initial state. However, it is important to note that the striking difference between the values of $R(t)$ is not restricted to this initial period, but extends to much longer times (which are, on the other hand, small compared to the time for quantum recurrences). In this respect our results indicate time-dependent quantum signatures of chaos of the mixed description which are beyond the well-known different time scales for the breakdown of quasiclassical approximations.

Finally we present the example for a quantum state prepared on a regular island embedded into chaotic regions of the mixed quantum-classical phase space (**C**, Fig. 11). The structure of the selected island is shown in the lower part of Fig. 8. For such a state the situation is specific due to the spreading of the quantum state out of the regular island. After some initial time in which the quantum dynamics probes the regular region of the mixed dynamics, the wave packet enters the region in which the mixed dynamics is chaotic. Correspondingly for an initial time interval we find that the agreement between the mixed and full quantum description is as good as expected for regular dynamics, whereas for long times the quantum system shows the typical behavior of a chaotic state. The latter feature is evident from the time dependence of the Bloch radius which is displayed in the lower part of Fig. 11 on a sufficiently large time scale.

V. CONCLUSIONS

(1) We compared the nonlinear dynamical properties of a coupled quasiparticle-oscillator system in a mixed quantum-classical description to the full quantum evolution of the model. Our results are related to the general question of how the idea of the Born-Oppenheimer approach to analyze complex systems by a stepwise quantization can be extended to a dynamical description. A more systematic investigation of this question using other model systems is certainly of interest in view of the widespread use of this approach.

(2) We demonstrated that the regular structures of the mixed quantum-classical description such as the fixed points and the presence of a separatrix are associated with the corresponding adiabatic approximation, in which the nonadiabatic couplings are switched off and integrable reference systems can be defined. Comparing the evolution of quantum wave packets to the mixed quantum-classical description, we found that regular structures of the mixed description can serve as a support for wave packet propagation in the fully quantized system in the adiabatic regime. This should be of interest for other systems to which a stepwise quantization must be applied due to their more complex structure, e.g., for the purpose of forecasting the qualitative properties of propagating wave packets using the mixed description as a reference system.

(3) Signatures of chaos in the mixed quantum-classical description were found in the full quantum evolution of the system. In analogy to previous results for systems with a proper classical limit, the breakdown of the quasiclassical approximation is enhanced for states prepared in a chaotic region of the phase space. On the other hand, the stronger quantum correlations between the subsystems of the fully quantized system, which were found in the chaotic region of the mixed description, persist even in the long-time evolution of the system, and are specific signatures of chaos in the mixed description.

(4) From the point of view of the Born-Oppenheimer quantization scheme, there are different possible sources of chaos in a mixed quantum-classical model system. Either the adiabatic potentials are sufficiently complex (nonlinear and couple more than one vibronic degree of freedom) to support chaotic motion even within the adiabatic approximation, or the chaos is due to nonadiabatic couplings. In the considered model the adiabatic potentials are one dimensional and thus manifestly integrable. Hence the observed quantum signatures of chaos are unambiguously related to nonadiabatic couplings. This mechanism should be of interest also for other systems treated by a stepwise quantization.

ACKNOWLEDGMENT

Financial support from the Deutsche Forschungsgemeinschaft (DFG) is gratefully acknowledged.

[1] E. J. Heller, *Chaos and Quantum Physics*, edited by M. J. Giannoni, A. Voros, and J. Zinn-Justin, Les Houches Summer School Sessions LII (North-Holland, Amsterdam, 1991).

[2] O. Bohigas, S. Tomsovic, and D. Ullmo, Phys. Rep. **223**, 43 (1993).

[3] W. P. Reinhardt, Prog. Theor. Phys. Suppl. **116**, 179 (1994).

[4] M. Born and R. Oppenheimer, Ann. Phys. (Leipzig) **84**, 457 (1927).

[5] G. Herzberg, *Electronic Spectra and Electronic Structure of Polyatomic Molecules* (van Nostrand, Princeton, 1966).

[6] P. Pechukas, Phys. Rev. **181**, 174 (1969).

[7] M. Born and K. Huang, *Dynamical Theory of Crystal Lattices*, (Clarendon, Oxford, 1954), Appendix VIII.
[8] R. Blümel and B. Esser, Phys. Rev. Lett. **72**, 3658 (1994); Z. Phys. B **98**, 119 (1995).
[9] A. Bulgac and D. Kusnezov, Chaos, Solitons, Fractals **5**, 1051 (1995).
[10] D. M. Leitner, H. Köppel, and L. S. Cederbaum, J. Chem. Phys. **104**, 434 (1996).
[11] M. Sonnek, H. Eiermann, and M. Wagner, Phys. Rev. B **51**, 905 (1995).
[12] R. Graham and M. Höhnerbach, Z. Phys. B **57**, 233 (1984).
[13] M. Kus, Phys. Rev. Lett. **54**, 1343 (1985).
[14] L. Müller, J. Stolze, H. Leschke, and P. Nagel, Phys. Rev. A **44**, 1022 (1991).
[15] B. Esser and H. Schanz, Chaos, Solitons, Fractals **4**, 2067 (1994); Z. Phys. B **96**, 553 (1995).
[16] H. Schanz and B. Esser, Z. Phys. B **101**, 299 (1996).
[17] K. Takahashi, Prog. Theor. Phys. Suppl. **98**, 109 (1989).
[18] P. B. Berman, E. N. Bulgakov, and D. D. Holm, Phys. Rev. A **49**, 4943 (1994).